Corey Murphy

Project Description:

The following white paper is a numerical evaluation of the Couette flow that determined the accuracy of the most recent OpenFOAM CFD software release, version 18.10. OpenFOAM is a CFD software package that can calculate fluid flow in three-dimensional space around objects and between surfaces. In order to determine the validity of OpenFOAM version 18.10, a Couette flow problem was developed to compare the exact solutions (White[1]) to the predicted numerical solutions to determine the predictive error of the OpenFOAM simulations. Couette flow is the flow of a fluid in the space between two plates, one of which is moving tangentially relative to the other. For this simulation, plate length was set to one meter and the plates were separated by a height of 0.25 (2h). Four simulations were run during this investigation. Two simulations were run with varying Reynolds numbers of $Re_h = 125$ and $Re_h = 1250$. The two final simulations included an increased upper wall velocity of 6.5 with a Reynolds number of $Re_h = 812.5$ and $B = 3.25$. One of the additional simulations utilized a pressure gradient of 0.5 while the other utilized a temperature gradient of 300K at the lower wall's surface to 420K at the upper wall's surface. The simulation which included a temperature gradient had a Prandtl number of $Pr = 0.71$ and an Eckart number of $E_c = 3.508e\text{-}4$.

Conclusion:

The numerical solutions obtained from the OpenFOAM simulations were approximately the exact solutions calculated using the Couette flow theory. On average, the numerical solutions obtained from the simulation ended with a near one percent error when compared with the exact solutions, which is considered accurate. All simulated solutions converged and the results generated were accurate, confirming that the most recent OpenFOAM 18.10 update is acceptable to use for future fluid flow calculations.

References:

[1] White, F. M., 1974, Viscous Fluid Flow, McGraw-Hill, Inc, New York, Ny

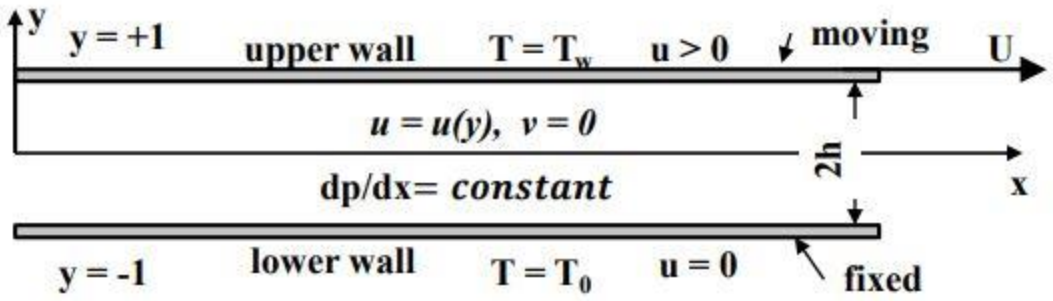

Figure 1: Sketch of Couette Flow Geometry

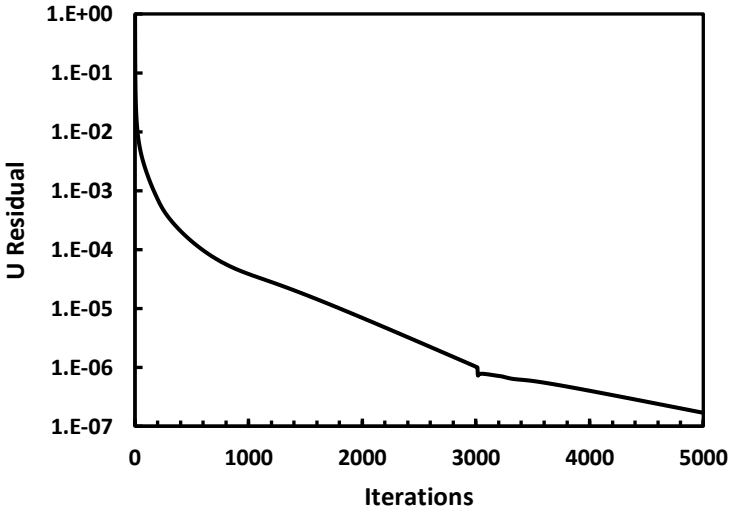

Figure 2: U-Velocity Convergence

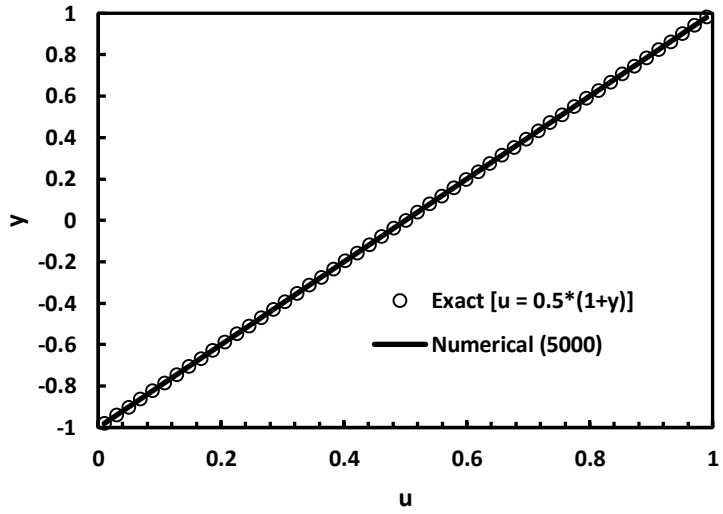

Figure 3: U-Velocity Profile

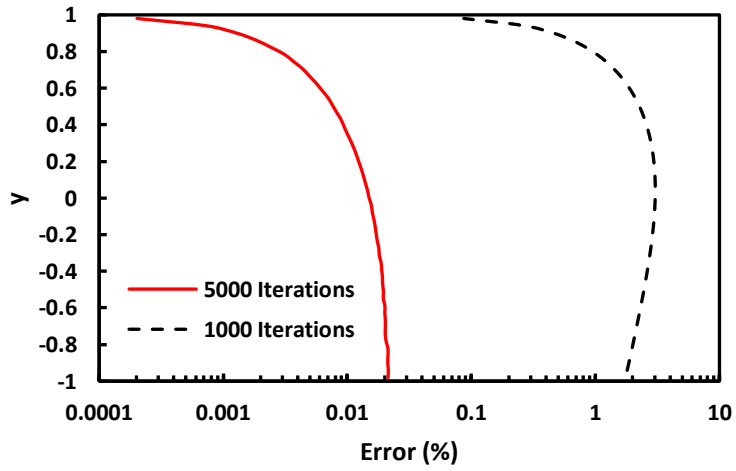

Figure 4: U-Velocity Error (Re = 125)

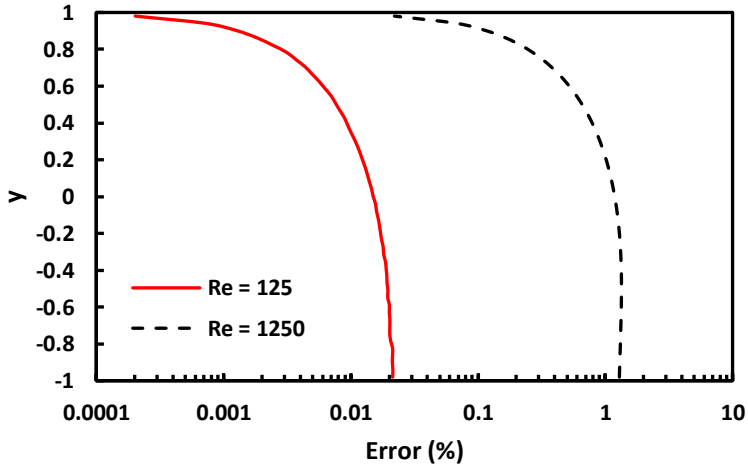

Figure 5: U-Velocity Error

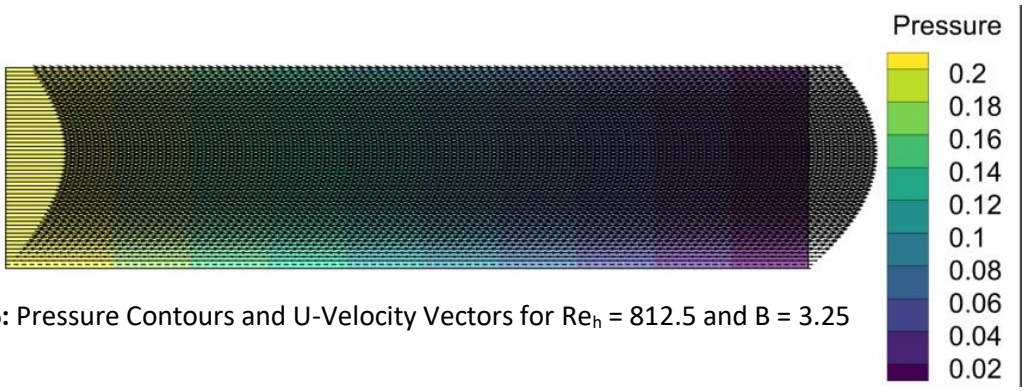

Figure 6: Pressure Contours and U-Velocity Vectors for Re_h = 812.5 and B = 3.25

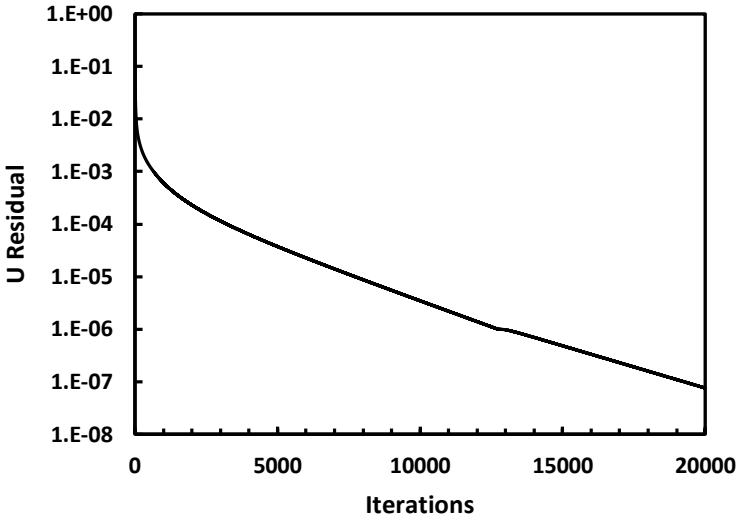

Figure 7: U-Velocity Convergence

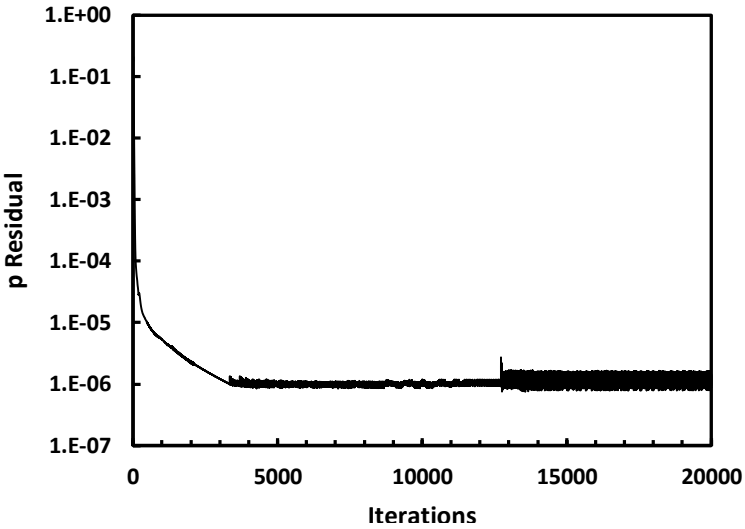

Figure 8: Pressure Convergence

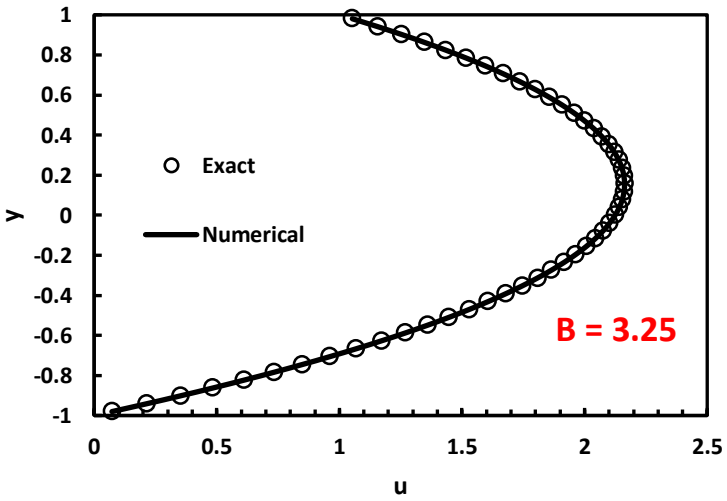

Figure 9: U-Velocity Profile

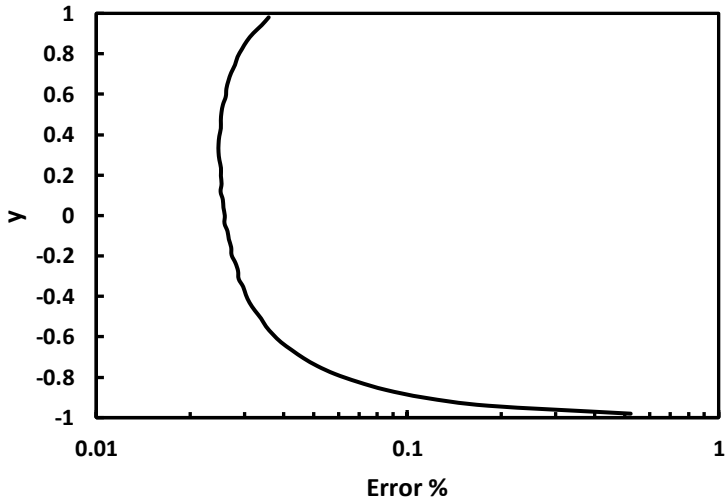

Figure 10: U-Velocity Error

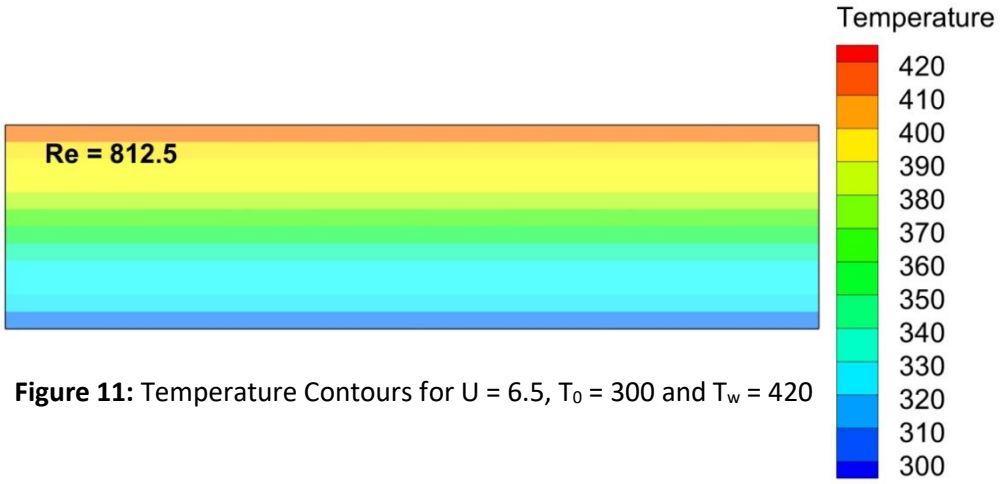

Figure 11: Temperature Contours for U = 6.5, T_0 = 300 and T_w = 420

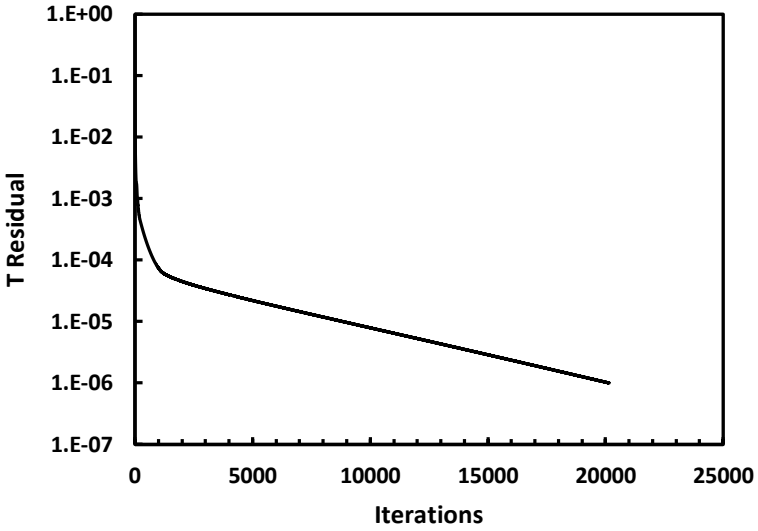

Figure 12: Temperature Convergence

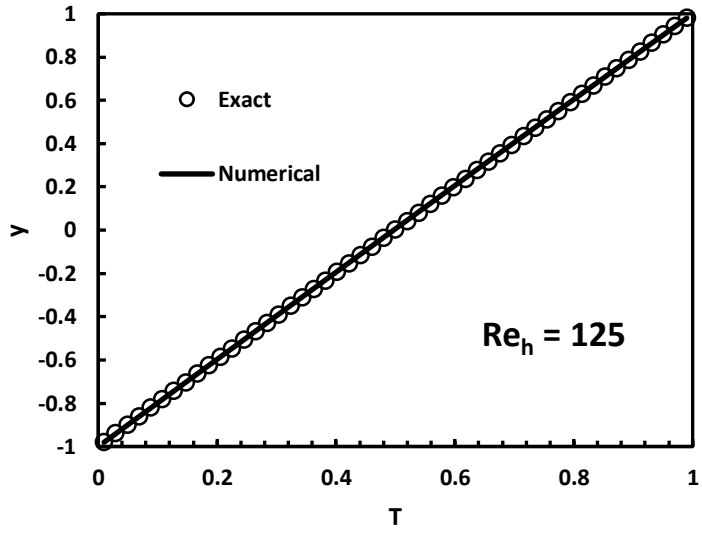

Figure 13: Temperature Profile

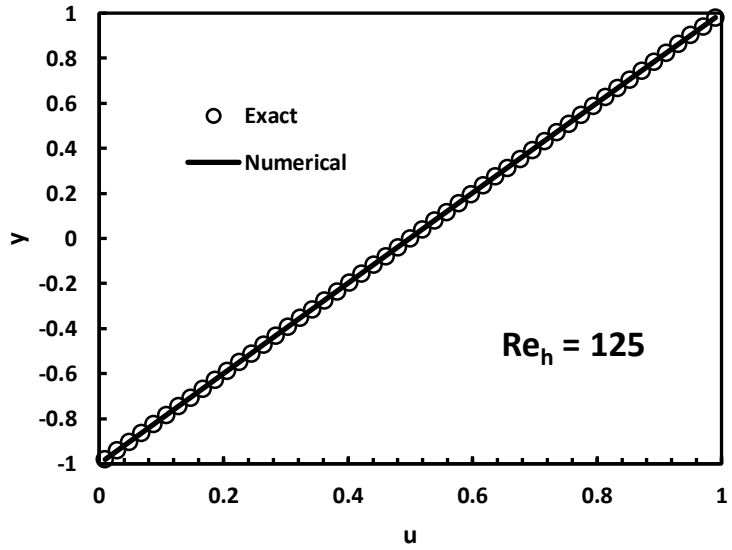

Figure 14: U-Velocity Profile

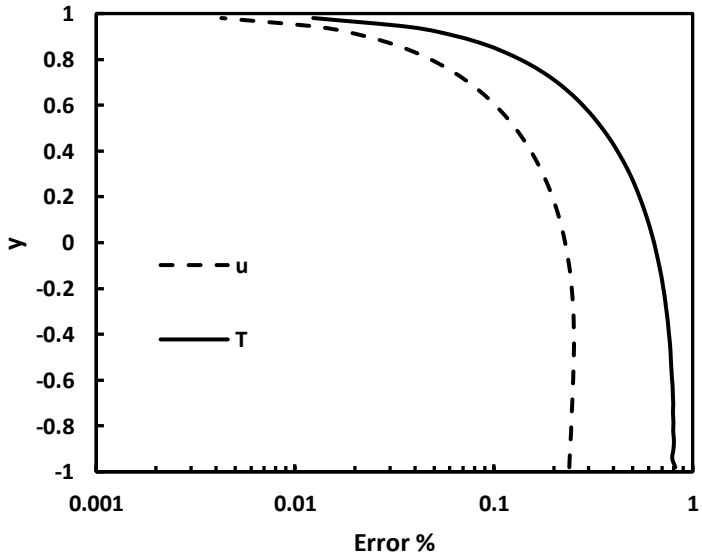

Figure 15: U-Velocity and Temperature Error

Corey Murphy

Project Description:

The following white paper is a numerical investigation of Poisuille flow that determined the accuracy of the most recent OpenFOAM CFD software release, version 18.10. In order to validate OpenFOAM, a Poiseuille flow problem was simulated and compared to the exact solutions (White[1]) to determine the predictive error of the OpenFOAM simulations. Poiseuille flow is the steady, axisymmetric flow in an infinitely long, circular pipe, caused by a constant pressure gradient (dp/dz) as seen in figure 1. For this simulation, the pressure gradient was set to (dp/dz) = 7.5, the pipe radius was set to r_0 = 0.1 m and the Reynold's number was set to Re_D = 290. The kinematic viscosity was calculated to be ν = 2.54e-03 using the above quantities. A single simulation was run over 20,000 iterations to verify convergence.

Simulation Results:

Figure 2 shows the convergence of the w-velocity over 20,000 iterations. Figure 3 shows the convergence of the pressure over 20,000 iterations. Both graphs converged at 1e-06, confirming the solution is solvable using OpenFOAM. Figure 4 shows the pressure contours and w-velocity vectors throughout the pipe at Re_D = 290. The pressure gradually dropped off from left to right along the z-axis. The velocity vectors of the fluid created a parabolic profile in the x-z and y-z plane. The difference in pressure along the pipe caused the fluid velocity to reach a maximum at the center of the pipe. Figure 4 plots the w-velocity profile for the numerical and exact solutions (White[1]) against each other over 20,000 iterations. The maximum and minimum w-velocity values are displayed on the plot. The exact solutions nearly mirror the profile of the numerical solutions obtained from the OpenFOAM simulation. Figure 5 displays the calculated percent error between the numerical and exact solutions for the w-velocity profile. The calculated error percentage was below one percent throughout the pipe.

Conclusion:

The numerical solutions obtained from the OpenFOAM simulations were close to the exact solutions. The numerical solutions obtained from the simulation ended with a percent error under one percent when compared with the exact solutions, which is considered accurate. All simulated solutions converged and the results generated were accurate, confirming that the most recent OpenFOAM 18.10 update is acceptable to use for future fluid flow calculations.

References:

[1] White, F. M., 1974, Viscous Fluid Flow, McGraw-Hill, Inc, New York, Ny

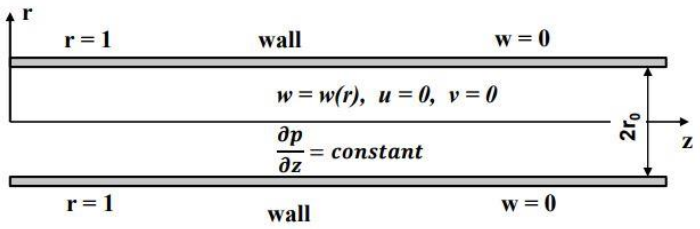

Figure 1: Sketch of the Poiseuille Flow Geometry

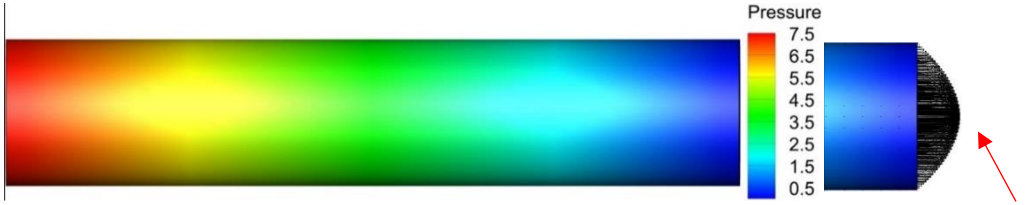

Figure 4: Pressure Contours and W-Velocity Vectors for Re_D = 290 **W_{max} = 7.350 m/s**

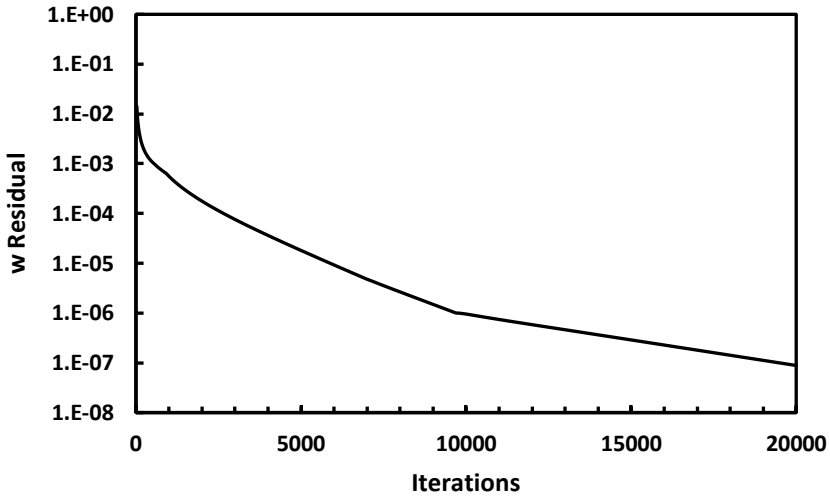

Figure 2: W-Velocity Convergence

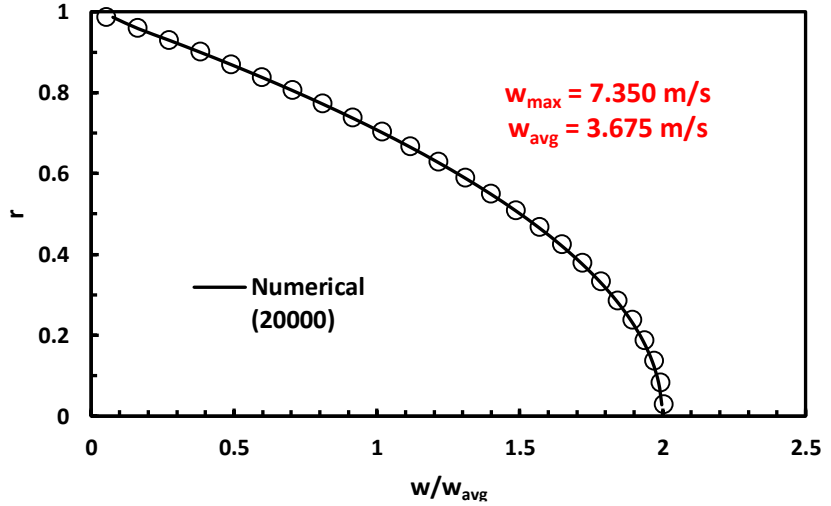

Figure 5: W-Velocity Profile

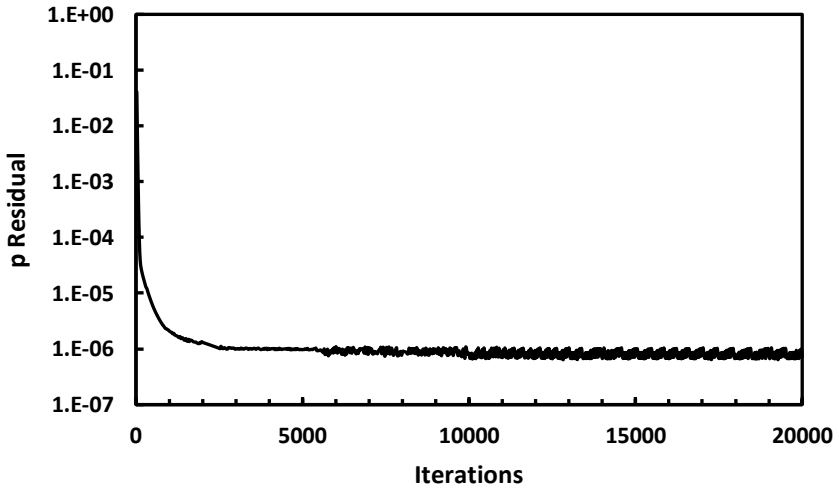

Figure 3: Pressure Convergence

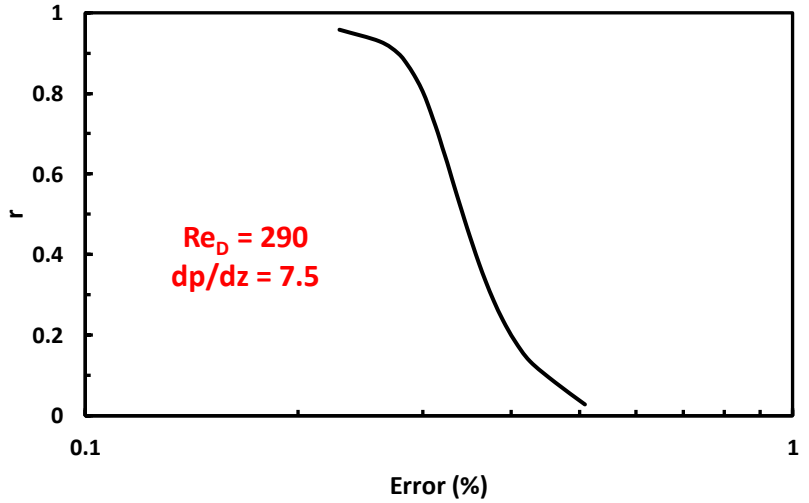

Figure 6: W-Velocity Error

Corey Murphy

Project Description:

The following white paper is a numerical investigation of Blasius flow that determined how the grid size in OpenFOAM version 18.10 effects truncation error. In order to accomplish this, multiple Blasius boundary layer problems were simulated using various grid sizes and compared to the exact solutions (White[1]) to determine the predictive error of the OpenFOAM simulations. A Blasius boundary layer describes the steady two-dimensional laminar boundary layer that forms along a flat plate which is held parallel to a constant unidirectional flow, as seen in figure 1. A total of 7 simulations were run at 7 different grid sizes using OpenFOAM. All simulations were conducted with a constant kinematic viscosity value of 5.45e-05.

Simulation Results:

Figure 2 shows the pressure contours of the pressure gradient from the simulation. This pressure gradient comes from the development of the flow. Figure 3 shows the convergence of the u-velocity from the 60x30 grid simulation. The u-velocity converges at 1e-06. Figure 4 shows the u-velocity profile at x = 2.4 m, simulated on a 60x30 grid. The numerical and exact solutions nearly mirror each other on the u-velocity profile plot. The percent error between the exact and numerical solutions for the 60x30 grid simulation was plotted up to the boundary layer thickness, δ_{99}. This is displayed in figure 5 which also includes the maximum and average error values that occurred. Table 1 shows the average and maximum error for the various grid sizes used in the simulation. The four grid sizes listed proved to be second order accurate for the Blasius boundary layer. Figure 6 illustrates the truncation error of the four second order accurate grid sizes that qualified as linear reductions of the given kinematic viscosity. The finest grid displayed on the plot is the 60x30 grid.

Conclusion:

The numerical solutions obtained from the OpenFOAM simulations moved closer towards the exact solutions as grid size increased. The numerical solutions obtained from the simulation utilizing the finest 60x30 grid ended with a percent error close to one percent when compared with the exact solutions, which is considered accurate. The four grid sizes listed in table 1 all proved to be second order accurate for the Blasius boundary layer. All simulated solutions converged and the results generated were accurate, confirming that truncation error decreases as grid size increases in OpenFOAM version 18.10

References:

[1] White, F. M., 1974, Viscous Fluid Flow, McGraw-Hill, Inc, New York, Ny

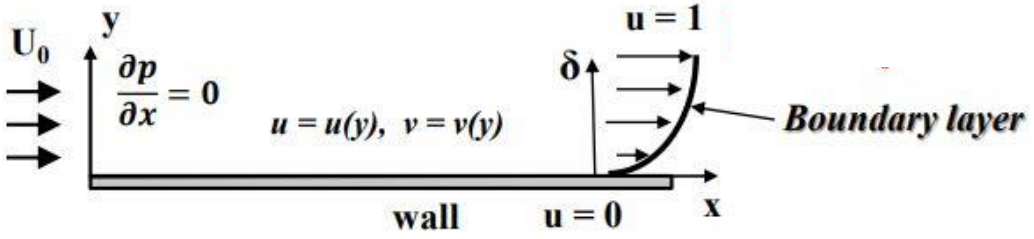

Figure 1: Blasius Flow Problem Sketch

Figure 2: Pressure Contours

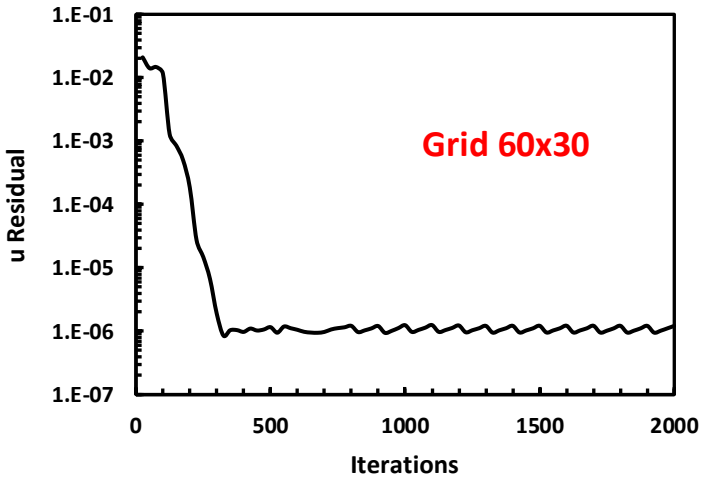

Figure 3: u-Velocity Convergence

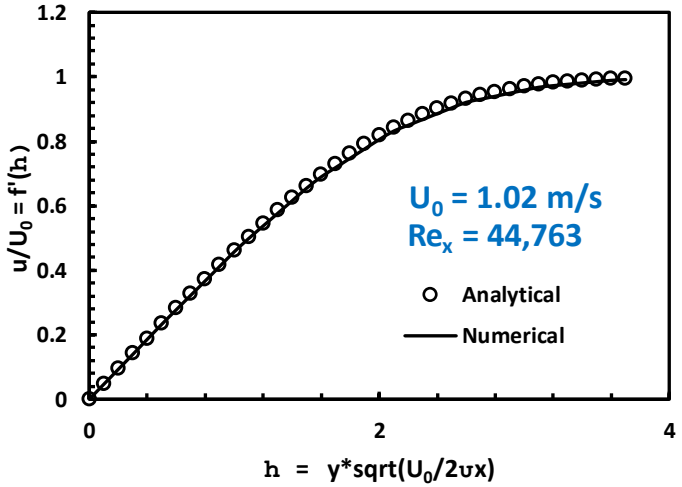

Figure 4: U-Velocity Profile (60x30 Grid)

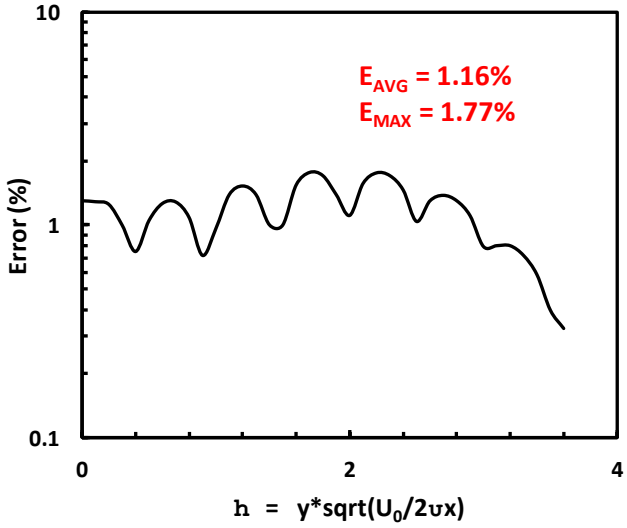

Figure 5: u-Velocity Error

Factor	Grid	E_{AVG}	E_{MAX}
1.00	30x15	4.72	7.70
1.33	40x20	2.54	4.25
1.67	50x25	1.76	2.84
2.00	60x30	1.16	1.77

Table 1: U-Velocity Error for Different Grids

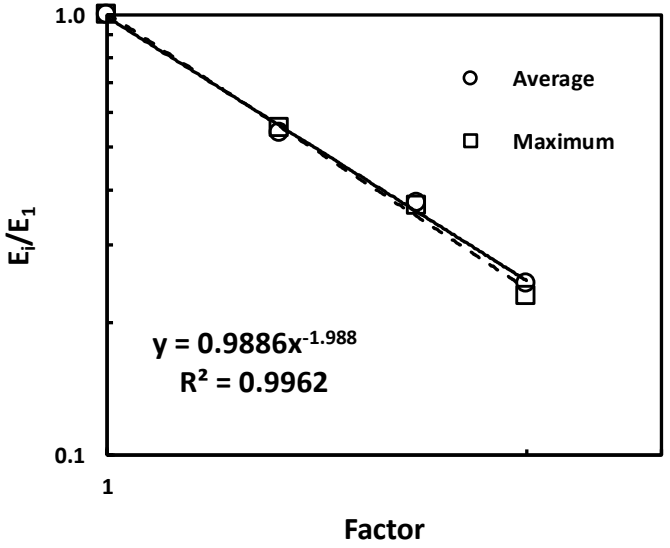

Figure 6: U-Velocity Error for Different Grids

Corey Murphy

Project Description:

The following white paper describes a simulation of Wedge Flow using OpenFOAM v18.10. The first set of simulations used the Falkner-Skan boundary layer. The Falkner-Skan boundary layer is a two-dimensional, steady, laminar flow of an incompressible fluid over an inclined plane as shown in Figure 1. These simulations investigated the effects of the boundary layer and symmetry of the wedge. One simulation was run using a full wedge while the other was run using the upper half wedge. Both simulations were conducted using a Reynolds number of $Re_x = 17{,}241$. The results from these simulations were used to compare to the analytical results (White[1]).

The second simulation investigated the vortex shedding that takes place behind the wedge. The periodic wedge flow simulation is a two-dimensional, unsteady, laminar flow of an incompressible fluid around a wedge. During these simulations, low pressure vortices continuously form and shed away from the wedge. The Strouhal number was calculated and compared to the given published data (Okamoto[2]). This simulation was conducted using a kinematic viscosity of v = 2.9412e-03 m^2/s and a Reynolds number of $Re_c = 3{,}400$. The results from this simulation were then compared to the analytical results (White[1]).

Simulation Results:

The first set of figures were compiled from the Falkner-Skan boundary layer simulations. Figure 2 shows the convergence of the u-velocity. The u-velocity converged at 1e-06, confirming that this is a steady problem. Figure 3 is a graphic of the pressure contours over the full wedge. Notice the stagnation point at the tip of the wedge where the flow separates. Figure 4 is a plot of the exact and numerical u-velocity profile for the full wedge. The numerical solution nearly mirrors the exact solution on this plot. Figure 5 is a plot of the u-velocity error for the full wedge simulation. The u-velocity error appears to decrease over the boundary, with the maximum error occurring at the beginning of the sample line. Figure 6 is a graphic of the pressure contours over the upper half wedge, which closely resembles the pressure contours of the full wedge. Notice the stagnation point at the angled section of the wedge where the flow separates. Figure 7 is a plot of the exact and numerical u-velocity profile for the upper half wedge. Similar to the full wedge, the numerical solution still nearly mirrors the exact solution for the upper half wedge. Figure 8 is a plot of the u-velocity error for the upper half wedge simulation. The u-velocity error appears to decrease over the boundary, with the maximum error occurring at the beginning of the sample line, resembling the full wedge error. Table 1 compares the average and maximum errors from both the full and upper half wedge simulations. Both average and maximum errors were nearly identical for the two different simulations, suggesting that the half wedge simulation can be used in substitution of the full wedge to decrease the overall running time of the simulation.

The second set of figures were compiled from the periodic wedge flow simulation. Figure 9 is a graphic of the pressure contours around the wedge at time T = 10 as well as the initial vortex pair that shed off the wedge. The lowest pressure area on the contour graphic occurs at the center of both vortices. These low-pressure vortices start to move away from the wedge with new vortices forming in their place. Figure 10 is a graphic of the pressure contours around the wedge at time T = 120 as well as three vortices that were shed off the trailing edge of

the wedge. The lowest pressure of each vortex occurs directly after shedding off the trailing edge of the wedge. The vortices begin to diffuse as the they move farther away from the wedge. Both Figure 11 and Figure 12 are plots that show the periodic base pressure. In the initial stage from T = 0 to approximately T = 30, shedding does not occur. Once the cyclical shedding commences, the frequency and pressure peaks remain consistent until T = 240. Notice the sinusoidal oscillation of the base pressure throughout the simulated time interval. Figure 13 is a plot that shows the amplitude (FFT of the base pressure) versus the dimensionless frequency. The Strouhal number, which represents the peak pressure point on the wedge, is displayed on this plot.

Conclusion:

The solutions generated from the first set of simulations using OpenFOAM v18.10 confirmed that the steady Falkner-Skan boundary layer simulation was accurate. It can also be confirmed that symmetry boundaries are an acceptable and more efficient way to simulate a full wedge Falkner-Skan boundary layer problem.

The solutions generated from the second simulation using OpenFOAM v18.10 confirmed that the unsteady periodic wedge flow simulation was accurate. The calculated Strouhal number of $S_t = 0.225$ falls well within the accepted range of $0.165 \leq S_t \leq 0.246$ (Okamoto[2]). All simulated solutions converged and the results generated were accurate, confirming that OpenFOAM v18.10 is acceptable for simulating both steady and unsteady flow around a wedge.

References:

[1] White, F. M., 1974, Viscous Fluid Flow, McGraw-Hill, Inc, New York, Ny

[2] Okamoto, T., Yagita, M. and Ohtsuka, K., "Experimental investigation of the wake of a wedge," Bulletin of JSME, 20, 323, (1977)

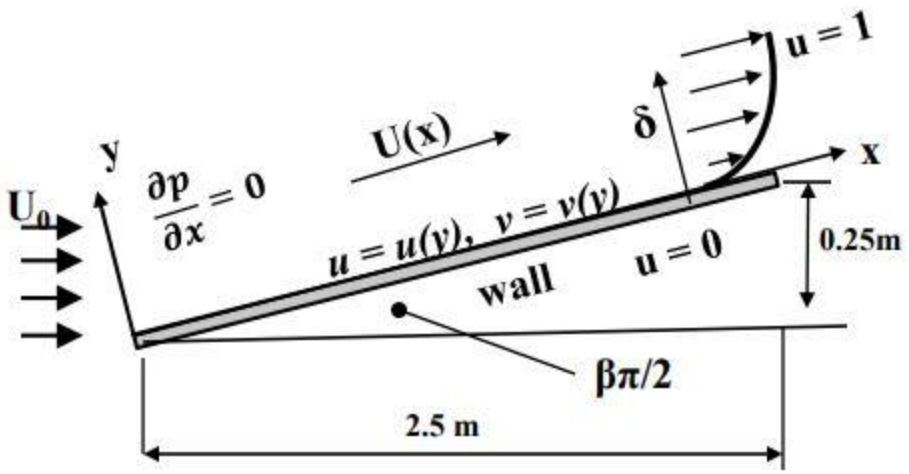

Figure 1: Falkner-Skan Flow Sketch

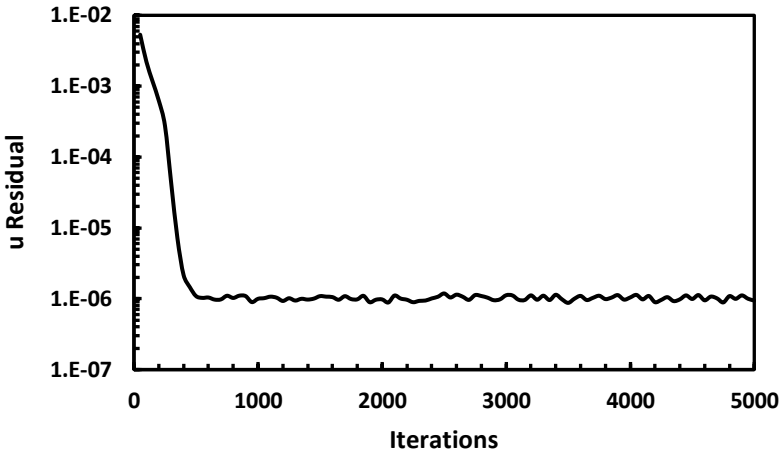

Figure 2: u-Velocity Convergence

Sample Line

DY = 0.002544 m

X_{end} = 2.3760 m

Y_{end} = 0.4805 m

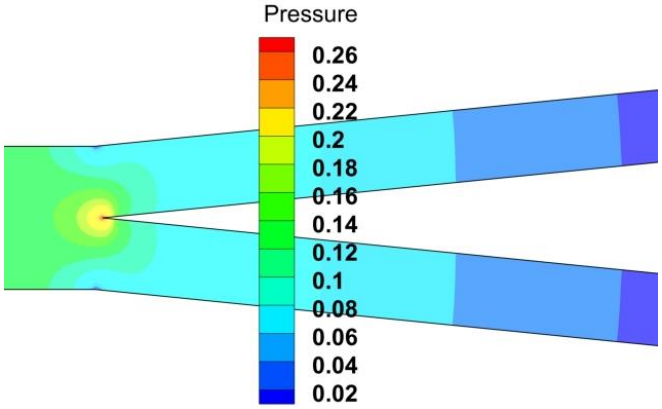

Figure 3: Full Wedge Pressure Contours

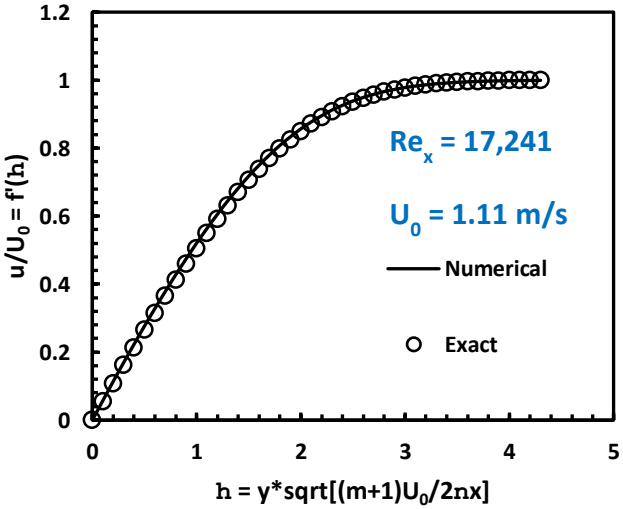

Figure 4: Full Wedge u-Velocity Profile

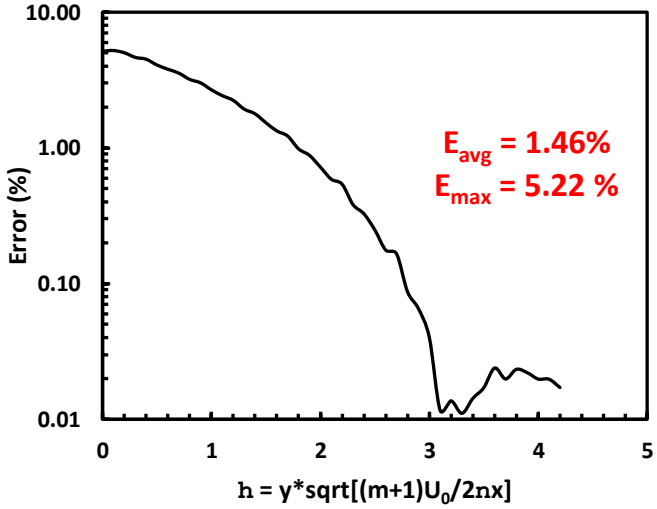

Figure 5: Full Wedge u-Velocity Error

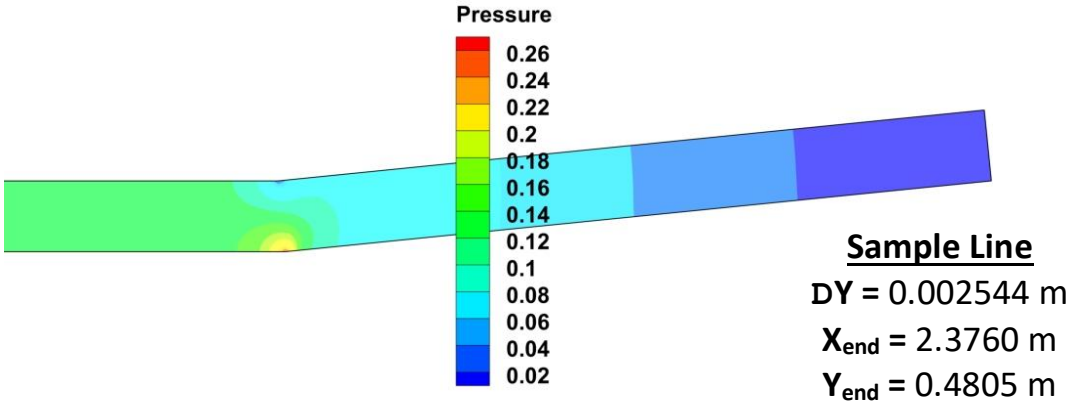

Figure 6: Half Wedge Pressure Contours

Table 1: Full Wedge vs. Half Wedge Error

Wedge	E_{AVG}	E_{MAX}
Full	1.45	5.21
Half	1.46	5.22

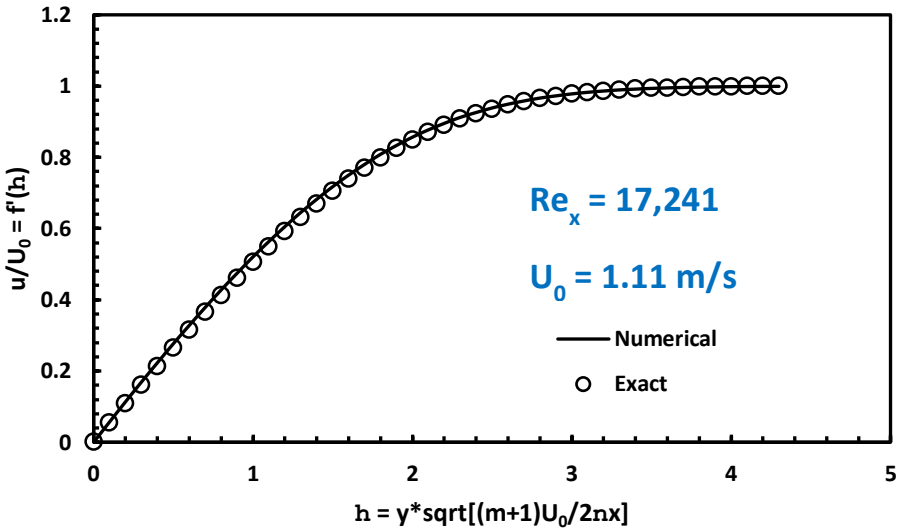

Figure 7: Half Wedge u-Velocity Profile

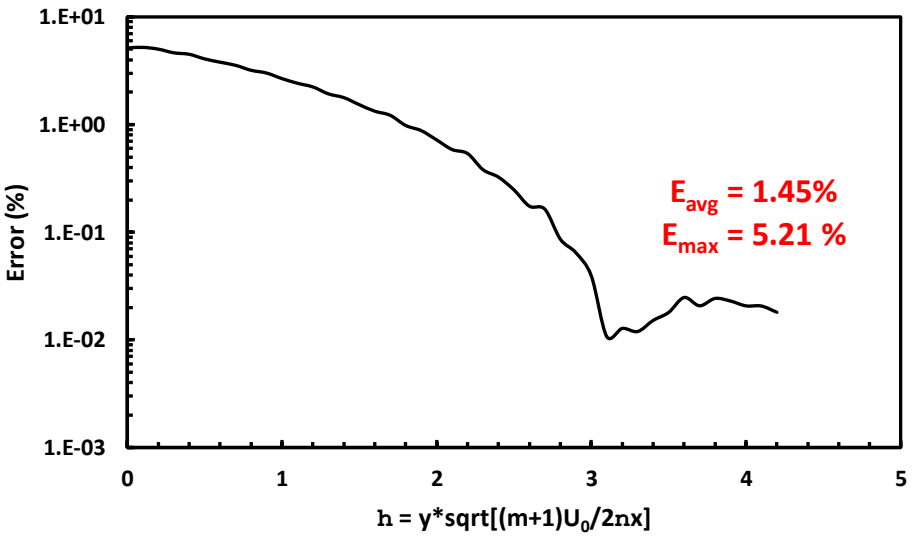

Figure 8: Half Wedge u-Velocity Error Percentage

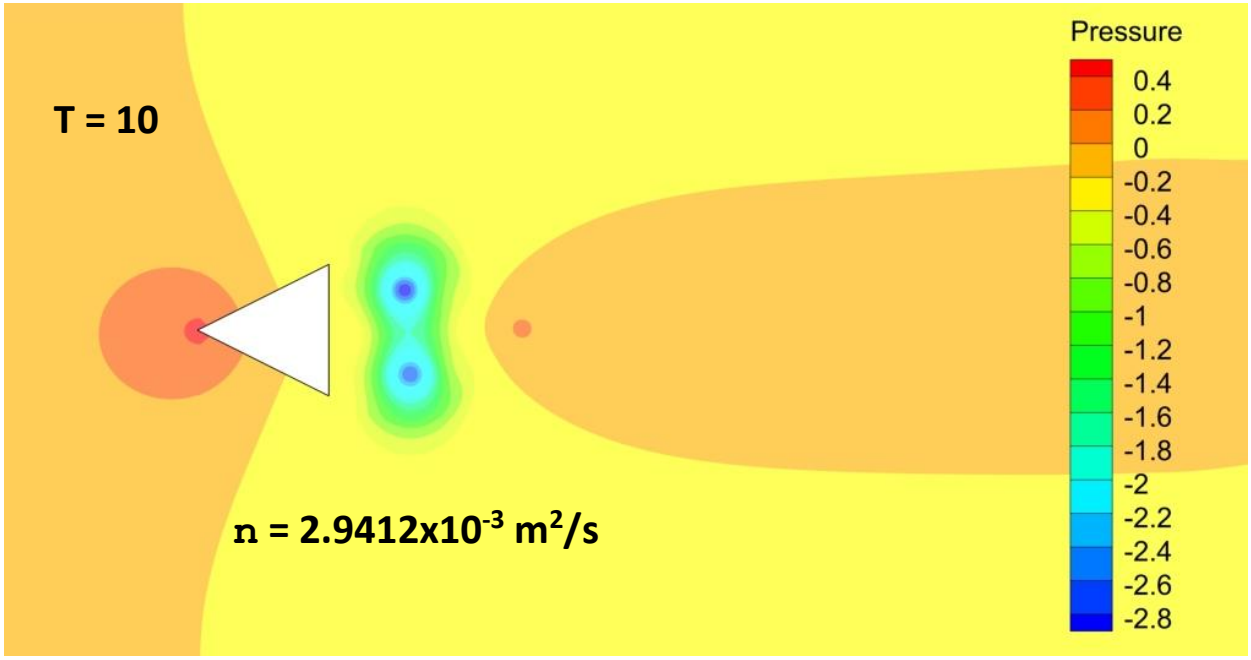

Figure 9: Pressure Contours for Vortex Shedding (T = 10)

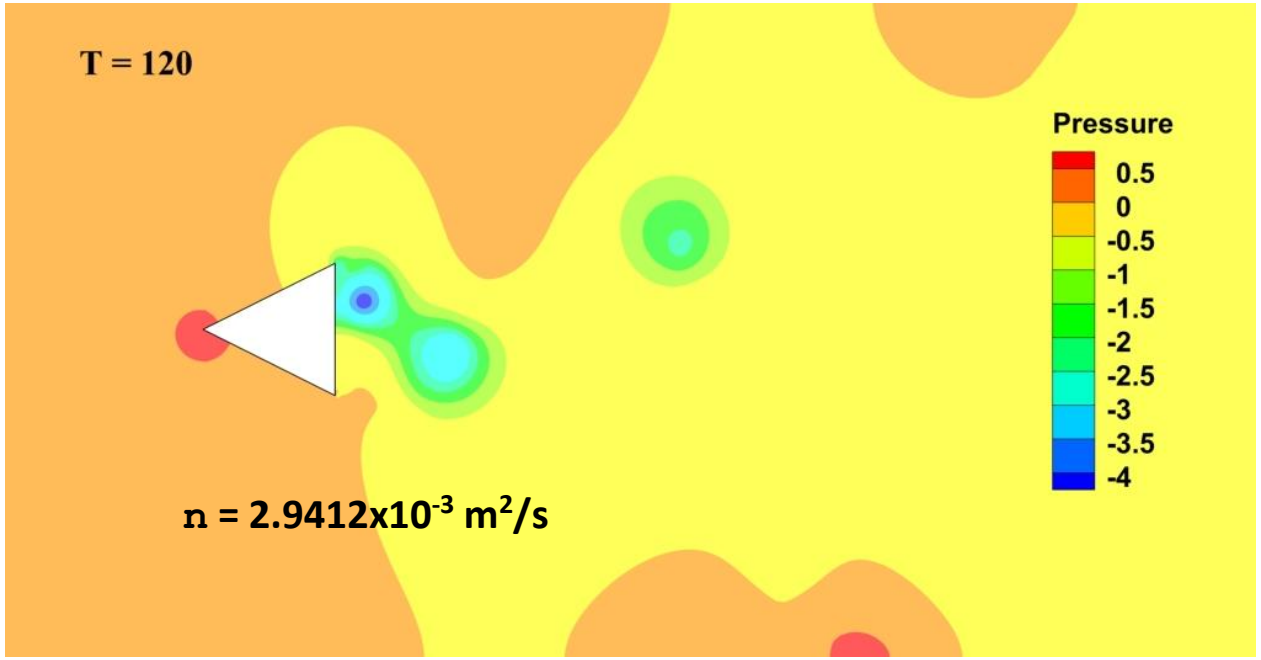

Figure 10: Pressure Contours for Vortex Shedding (T = 120)

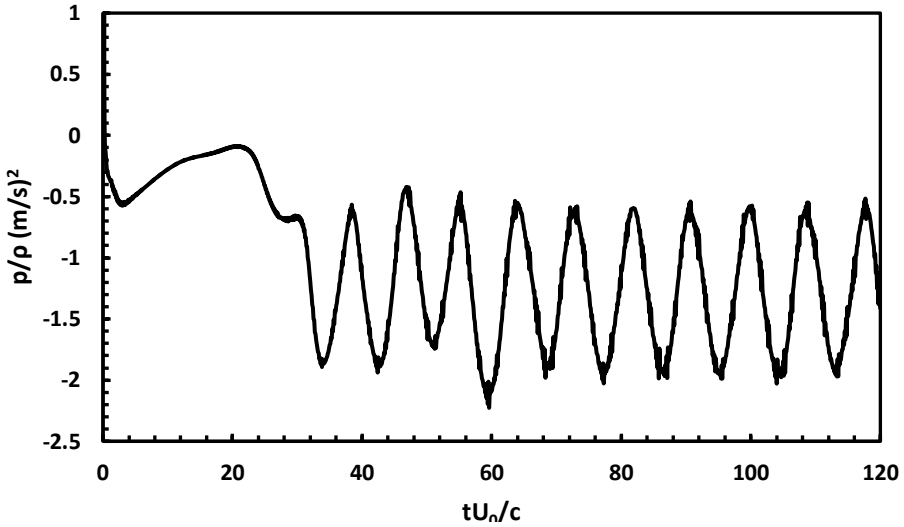

Figure 11: Initial Periodic Base Pressure

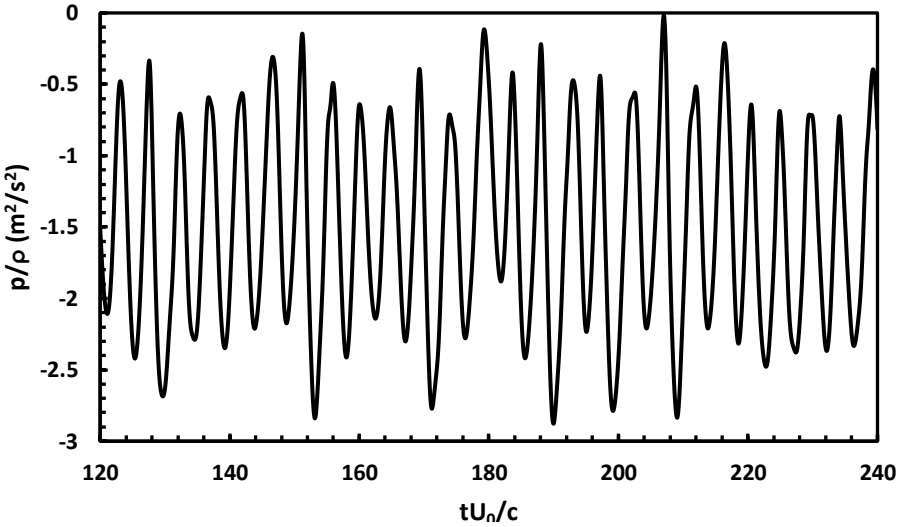

Figure 12: Full Periodic Base Pressure

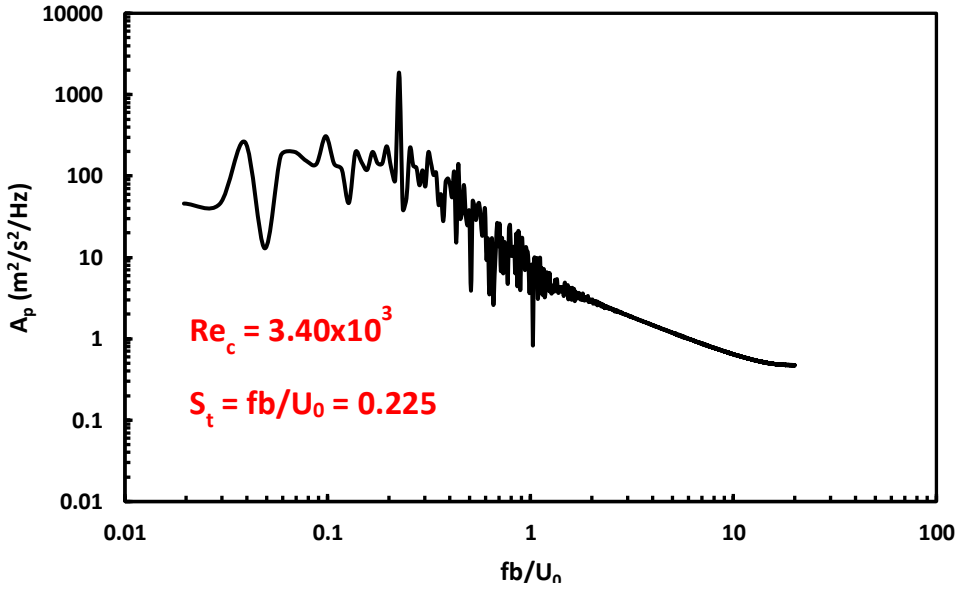

Figure 13: Discrete Fourier Transform of Base Pressure Data

Corey Murphy

Project Description:

The following white paper describes a simulation of nozzle flow using OpenFOAM v18.10. A nozzle flow is the two-dimensional, steady and laminar flow of a compressible fluid through a converging-diverging boundary, as shown in Figure 1. The simulation investigated the shock which was generated by the nozzle. The solutions calculated from this simulation were then compared to the analytical solutions (White[1]).

Solution Procedure:

The nozzle geometry was based on the NASA Model which can be seen in Figure 1. For the purpose of the OpenFOAM simulation, only the upper half of the nozzle was used. A symmetry plane was utilized for the bottom face. The length of the nozzle was L = 0.254 m and the height from the x-axis to the top of the nozzle at the outlet was h = 0.025 m. A 100x60 grid was used for this simulation. The inlet total pressure and outlet static pressure values were $p_{o\ inlet}$ = 11000 Pa and p_{outlet} = 8600 Pa respectively.

Solution Description:

Figure 2 is a graphic that displays the contours of the Mach number from the throat of the nozzle to the outlet of the nozzle. Figure 3 is a plot of the Mach number throughout the nozzle. As the flow leaves the throat and heads towards the outlet, the Mach number increases to a supersonic maximum of 1.42. Directly after this maximum is reached, the shock is generated, which caused the Mach number to rapidly decrease back to a subsonic value of approximately 0.70. The Mach number continues to slowly decrease as the flow moves toward the outlet of the nozzle. Figure 4 is a plot of the stagnation pressure throughout the nozzle. The stagnation pressure remains constant until the shock occurs. Once this happens, the stagnation pressure drastically drops and then immediately recovers to a new stagnation pressure value. Figure 5 is a plot of the stagnation temperature throughout the nozzle. The stagnation temperature remains constant until the shock is generated. At this moment, there is a small spike in stagnation temperature due to the pressure drop before it returns to its original value. Table 1 compares Mach number and stagnation values before and after the shock. A control volume analysis was completed to compare the results to the predicted values from OpenFOAM after the shock. The error percentages for these values when compared with the control volume analysis are displayed in the table.

Conclusion:

The solutions generated from the OpenFOAM simulation for both the pressure and stagnation pressure values produced minimal error when compared with the analytical solutions. The Mach number simulation results produced an error close to five percent when compared with the analytical solutions. Although not ideal, an error below five percent is acceptable. In order to reduce the predictive error for the Mach number, a larger grid size could be explored. This confirms that OpenFOAM v18.10 can accurately simulate a nozzle flow for future simulation purposes.

References:

[1] White, F. M., 1974, Viscous Fluid Flow, McGraw-Hill, Inc, New York, Ny

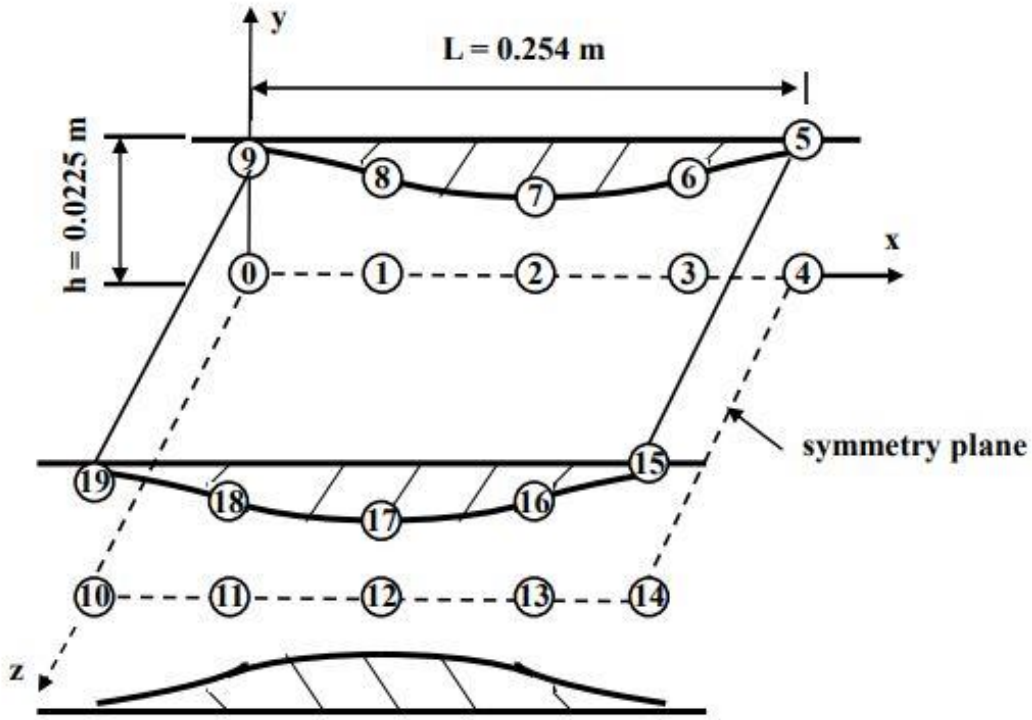

Figure 1: Problem Sketch of NASA Model

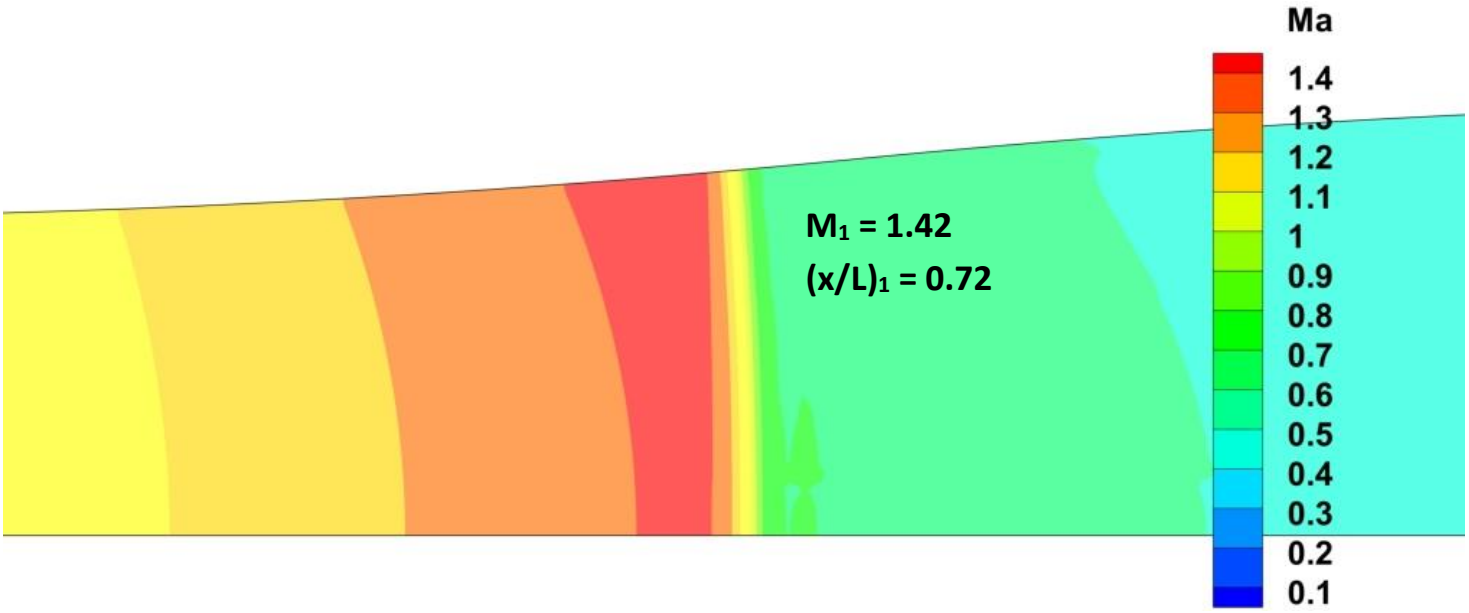

Figure 2: Mach Number Contours in Nozzle

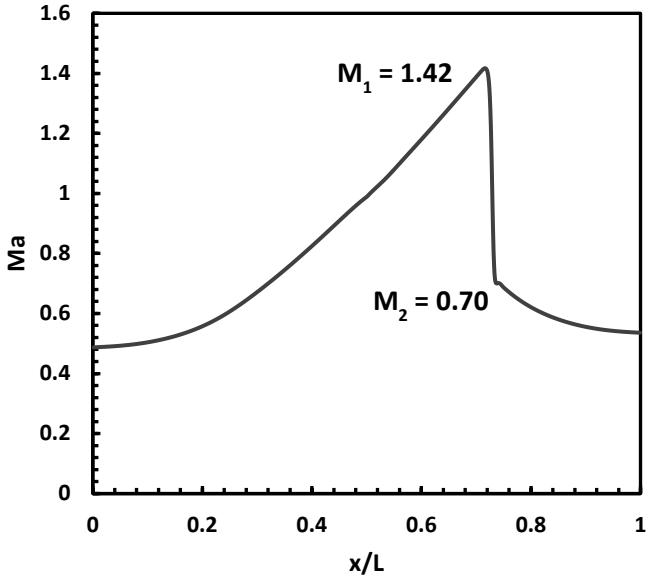

Figure 3: Mach Number Throughout Nozzle

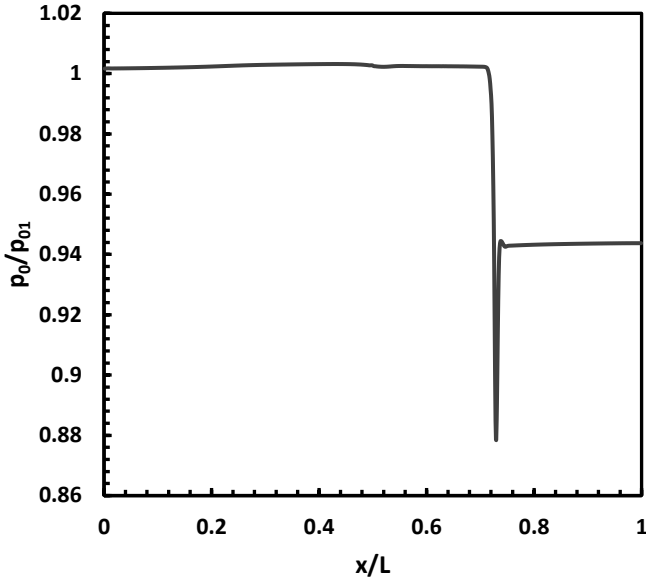

Figure 4: Stagnation Pressure Ratio

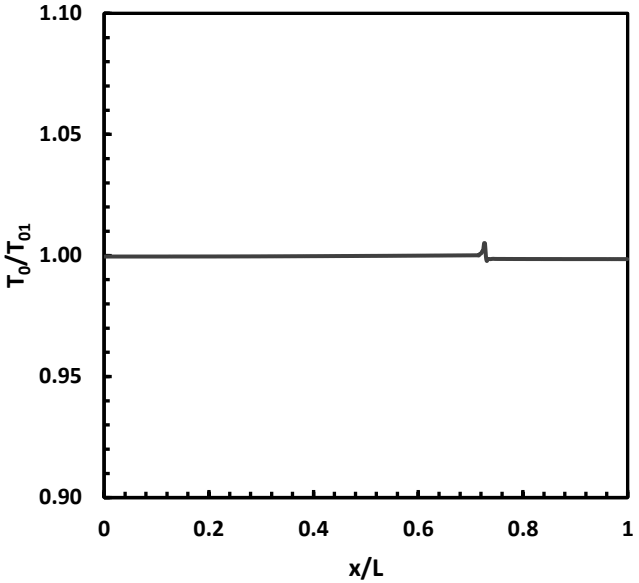

Figure 5: Stagnation Temperature Ratio

Table 1: Values Before vs. After Shock

Property	Sta 1	Sta 2		Error (%)
		Predicted	CVA	
Ma	1.42	0.70	0.73	4.30
p/p_1	1.00	2.22	2.18	1.84
p_0/p_{01}	1.00	0.94	0.95	1.04

Corey Murphy

Project Description:

The following white paper describes multiple simulations of turbulent channel flow using OpenFOAM v18.10. Turbulent channel flow is a two-dimensional, steady, turbulent flow between two infinitely long parallel plates as shown in Figure 1. These simulations were run to test and compare two different turbulence models that predict the mean turbulent flow through a channel. The results from these two model simulations were then compared to the analytical Spalding expression (White[1]). The first turbulence model tested was the Spalart-Allmaras turbulence model. The first simulation was run using a uniformly spaced grid to confirm the convergence of the u-velocity and turbulent eddy viscosity. Four more simulations were run using non-uniformly spaced grids with various grid factors. The predictive error norms corresponding to each grid factor were calculated to determine the effectiveness of increasing the grid factor of the non-uniform grids. The second turbulence model tested was the K-ω turbulence model. One simulation was run using the final non-uniform grid from the Spalart-Allmaras turbulence model simulation. All simulations were run to replicate Laufer's experimental measurements with a Reynolds number of $Re_h \approx 12{,}300$ (White[1]).

Solution Procedure:

The simulated channel displayed in Figure 1 was comprised of two infinitely long parallel plates. The height from the x-axis to the surface of the plate wall was h = 0.0635 m. The height from the surface of the bottom plate to the surface of the upper plate was 2h = 0.127 m. The target maximum velocity was calculated to be $U_0 = 4.65$ m/s. All grids had inflow and outflow boundaries set to cyclic. A pressure gradient of zero was used throughout the channel. All simulations were run using a kinematic viscosity of $\upsilon = 2.40\text{e-}05$ m^2/s^2.

The first Spalart-Allmaras simulation was run using a uniform, two block 100x60 grid. This simulation was used to confirm the convergence of the u-velocity at 1e-04 and the turbulent eddy viscosity at 1e-03. The next four simulations were run using non-uniform, two block 100x60 grids with grid factors of 5, 10, 20 and 30. The function used for these simulations was simpleFoam and the Reynolds-Averaged Navier-Stokes Model was set to SpalartAllmaras in the turbulenceProperties file. In order to achieve the target Reynolds number of $Re_h \approx 12{,}300$ for each different grid factor, the U_{bar} value needed to be adjusted in the fvOptions file before each simulation.

The K-ω turbulence model simulation was run using the final non-uniform grid from the Spalart-Allmaras turbulence model simulations. This grid was the non-uniform, 100x60 two block grid that used a grid factor of 30. The function used for this simulation was simpleFoam and the Reynolds-Averaged Navier-Stokes Model was set to kOmega in the turbulenceProperties file. U_{bar} was once again adjusted in the fvOptions file in order to achieve the target Reynolds number.

Simulation Results:

The first set of figures were compiled from the Spalart-Allmaras turbulence model simulations. Figure 2 is a plot of the u-velocity residuals for the uniform 100x60 grid. The u-velocity converges at approximately 1e-04. The maximum and bulk velocities are displayed on the plot. Figure 3 is a plot of the turbulent eddy viscosity residuals for the uniform 100x60 grid.

The turbulent eddy viscosity converges at approximately 1e-03. Figure 4 is a plot comparing the turbulent boundary layer velocity profile from the Spalart-Allmaras turbulence model to the Spalding expression. The results from this simulation used the final non-uniform grid factor of 30 and met the three turbulent boundary layer requirements. The Spalding solution nearly mirrors the numerical Spalart-Allmaras solution. Table 1 includes the Spalding expression error norms for various grid factors. Notice the error norms decrease as the grid factor increases. Table 2 is a list of the initial twelve y+ values off the wall from the final non-uniform grid simulation.

The second set of figures were compiled after completing the K-w turbulence model simulation. Figure 5 is a plot comparing the turbulent boundary layer velocity profile from the K-w and Spalart-Allmaras turbulence models to the Spalding expression. All three models have profiles that nearly mirror each other. Figure 6 plots the turbulent eddy viscosity versus the y+ values for the Spalart-Allmaras and K-w turbulence models as well as the Spalding expression. The K-w turbulence model has turbulent eddy viscosity values that are below those of the Spalart-Allmaras turbulence model and Spalding expression for y+ values lower than 10. The three models eventually converge together and nearly mirror each other for y+ values greater than 10. Table 3 compares the values obtained from the Spalart-Allmaras turbulence model simulation to the values obtained from the K-w turbulence model simulation. Both models have similar values but notice the slightly smaller friction factor values for the K-w turbulence model.

Conclusions:

The comparison of the solutions generated from the Spalart-Allmaras turbulence model simulations confirmed that non-uniform grids are more accurate for simulating a turbulent channel flow. It can also be confirmed that larger grid factors yield more accurate turbulent boundary layer predictions. As the grid factor was increased, the predictive error norms decreased. The final grid factor of 30 satisfied the turbulent boundary layer requirements, confirming an accurate prediction.

The solutions generated from the Spalart-Allmaras turbulence model final non-uniform grid simulation and the K-w turbulence model simulation confirm that both models are acceptable for simulating a turbulent channel flow. The u-velocity and turbulent eddy viscosity profiles for both models nearly mirrored each other as well as the Spalding expression. Both models also had calculated values that were nearly identical. All simulated solutions converged and the results generated were accurate, confirming that the Spalart-Allmaras and K-w turbulence models can accurately predict a turbulent channel flow using OpenFOAM v18.10.

References:

[1] White, F. M., 1974, Viscous Fluid Flow, McGraw-Hill, Inc, New York, Ny

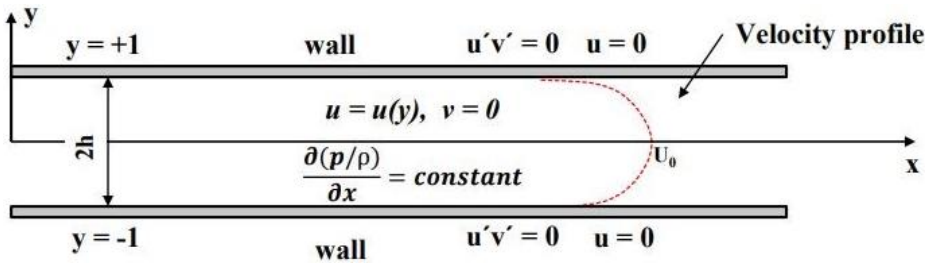

Figure 1: Turbulent Channel Flow Problem Sketch

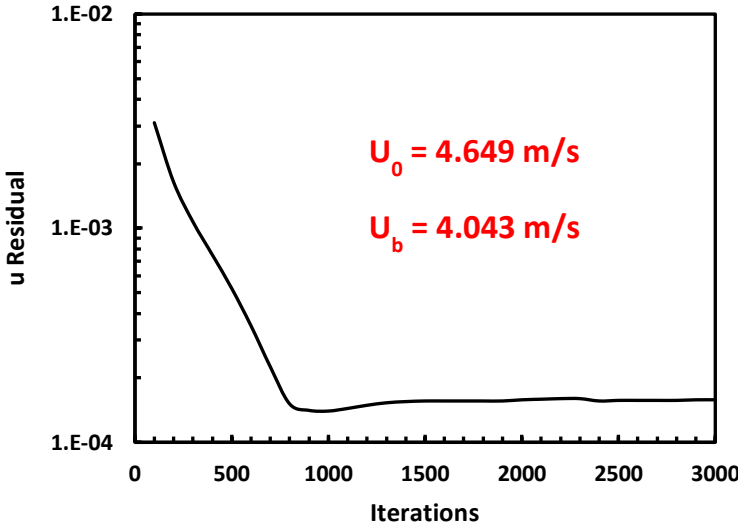

Figure 2: u-Velocity Converge

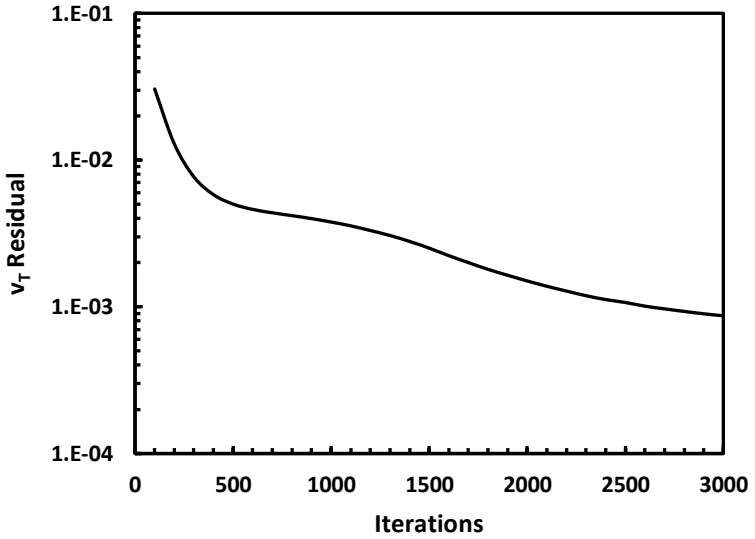

Figure 3: Turbulent Viscosity Convergence

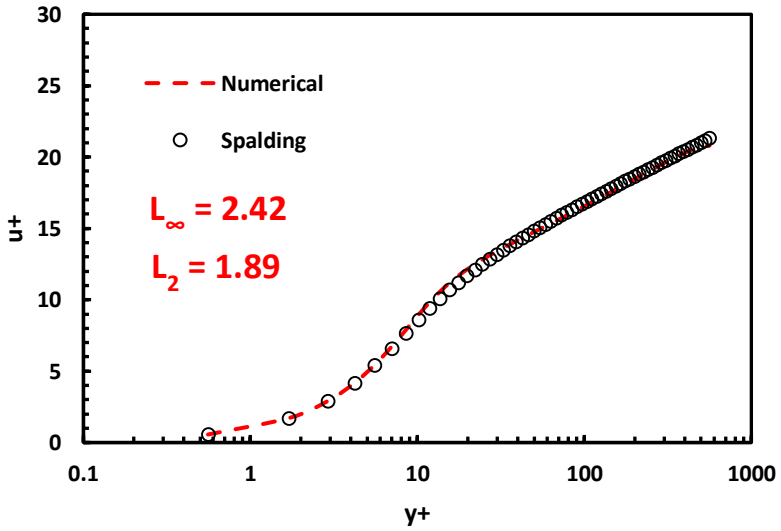

Figure 4: TBL Velocity Profile SA Model

Table 1: Error Norms for Various Grid Factors

	Error (100x120 Grid)	
Factor	Spalding	
	L_2	L^∞
1	4.1	6.97
5	3.05	4.34
10	1.73	2.9
20	1.79	2.59
30	1.89	2.42

Table 2: Initial y+ Values

y+
0.557263
1.703658
2.919256
4.205877
5.569896
7.014045
8.544696
10.16549
11.88281
13.70211
15.62885
17.67124

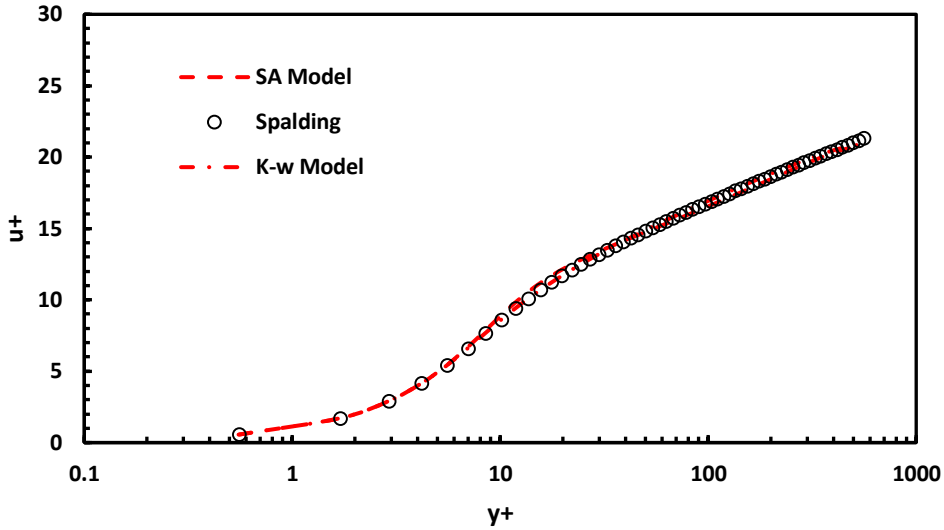

Figure 5: TBL Velocity Profile for SA and K-ω Model

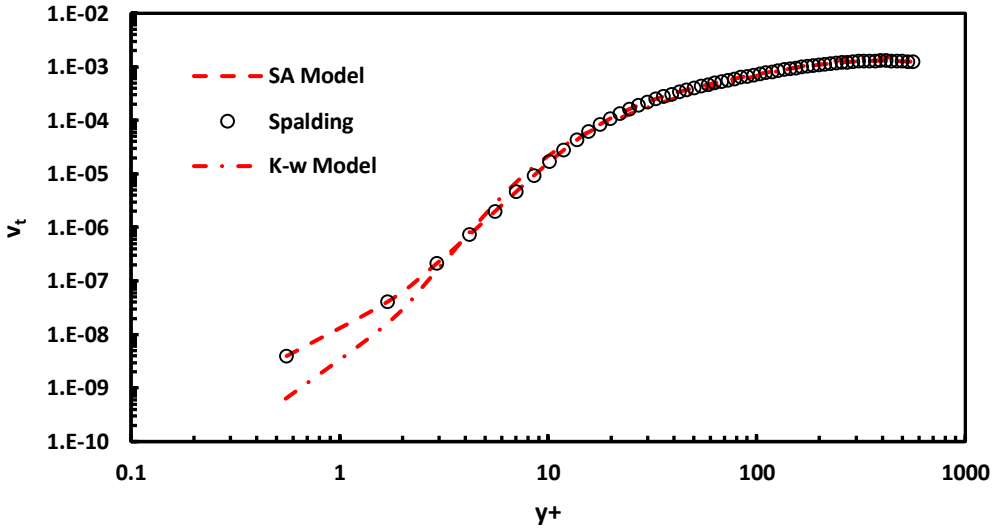

Figure 6: v_t vs y+ for SA and K-ω Model

Table 3: Spalart-Allmaras vs K-ω Turbulence Model Values

T Model	U_b (m/s)	U_a (m/s)	Re_h	u_τ (m/s)	Λ	Λ (log law)
SA	4.46	4.54	12024	0.219	0.0177	0.0185
Kw	4.45	4.52	11951	0.216	0.0173	0.0183

Corey Murphy

Project Description:

The following white paper describes a simulation of laminar flow passed a circular cylinder using OpenFOAM v18.10. This type of flow problem is an unsteady, incompressible, laminar flow over a cylinder as shown in Figure 1. The results obtained from the simulation were then compared to the experimental values (White[1]). A Reynolds number of $Re_D = 200$ was used for the simulation with a viscosity of $\upsilon = 7.50e\text{-}03\ m^2/s$.

Solution Procedure:

The cylinder flow problem was set up using two cylinders as shown in Figure 1. The diameter of the inner cylinder was D = 1.35 m and the dimension of the outer boundary was 12D = 16.2 m. The grid dimension was set to be 200x100 in the radial and tangential directions respectively. All boundaries were set to walls as the type. The uniform inlet velocity was set to v = 1.11 m/s in the x-direction with a pressure gradient of zero. The outlet boundary was set to have a uniform pressure of zero and a velocity gradient of zero. A uniform velocity of zero was applied along the walls of the cylinder.

The initial simulation's time interval was set from t = 0 to t = 125. Within the controlDict file, a probe was set to record base pressure. The probe was positioned on the centerline on the downstream side of the cylinder at 0.685 m. The function pisoFoam was used to execute the initial simulation. The final simulation's time interval was set from t = 125 to t = 225. This simulation was completed to determine the lift and drag coefficients as well as bubble length. The controlDict file was updated with relevant equations (White[1]) to accomplish this and a sampleDict file was added to record data on the downstream side. The function pisoFoam was once again used to execute the final simulation. Microsoft Excel was used to compile, analyze and plot the data acquired from OpenFOAM and Tecplot360 was used to create mesh and vorticity graphics.

Simulation Results:

Figure 2 is a graphic that displays the overall grid structure used in this simulation. Figure 3 is a graphic that displays a close-up view of the mesh surrounding the cylinder. Figure 4 is a plot of the initial periodic base pressure over the initial dimensionless time interval. The simulation properties are displayed next to this plot. Figure 5 is a pressure graphic of the vortex street at time t = 225. Notice the stagnation point at the leading edge of cylinder where the flow separates. The low-pressure vortices shed off the cylinder in an oscillatory manner. Figure 6 is a graphic that displays the z-vorticity contours around the cylinder and the angle of separation, θ_s. Similar to Figure 4, Figure 7 is a plot that depicts the final periodic base pressure when the flow was developed over the final dimensionless time interval. Notice the periodic oscillations of the base pressure over the entire dimensionless time interval. The average base pressure value, p_{pB}/ρ, and the base pressure coefficient, $-C_{pB}$, are also displayed on this plot. Figure 8 plots the amplitude versus the dimensionless frequency for the base pressure. To compile this plot, an FFT of the base pressure was computed to determine the amplitude and frequency. A frequency was related to the maximum amplitude to determine the Strouhal number of $S_t = 0.21$, which represents the peak pressure point on the cylinder. Figure 9 is a plot of the coefficient of drag over the final dimensionless time interval. Notice the oscillatory behavior of the drag coefficient

over the entire final dimensionless time interval which is a result of the recirculation zone. Figure 10 is a plot of the u-velocity profile at time t = 225. Depicted on the plot is the bubble length, ℓ_c, which is the point where the recirculation zone ends. Table 1 compares the laminar cylinder flow experimental parameters (White[1]) to the parameters generated through the OpenFOAM simulation. The coefficient of drag simulation value and the bubble length simulation value were slight outliers.

Conclusion:

The results generated from the OpenFOAM laminar cylinder flow simulation proved the overall goal of the simulation to create an accurate prediction. A majority of the simulation parameters were close to the given experimental parameters. The coefficient of drag simulation value proved to be an underestimate and the bubble length simulation value proved to be an overestimate when compared with their respective experimental values. The experimental values cannot be taken as exact, therefore it can be said that all predicted values were relatively accurate. Further refinements to the 200x100 grid could lead to improved accuracy in these simulation parameters. It can be confirmed that the OpenFOAM simulation is an accurate representation of laminar flow passed a circular cylinder.

References:

[1] White, F. M., 1974, Viscous Fluid Flow, McGraw-Hill, Inc, New York, Ny

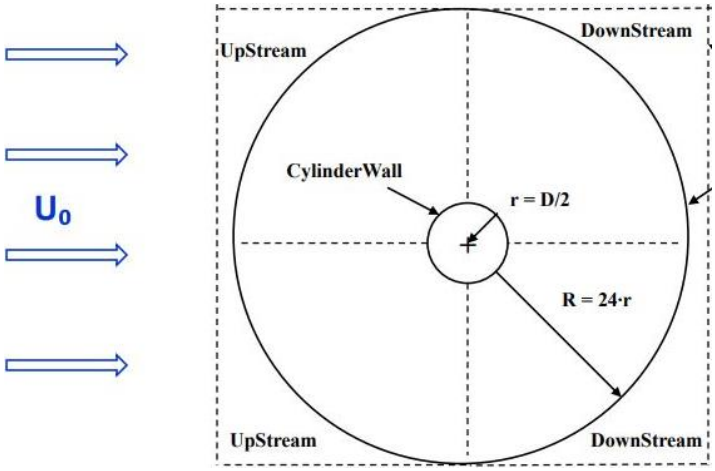

Figure 1: Laminar Flow Past a Circular Cylinder Sketch

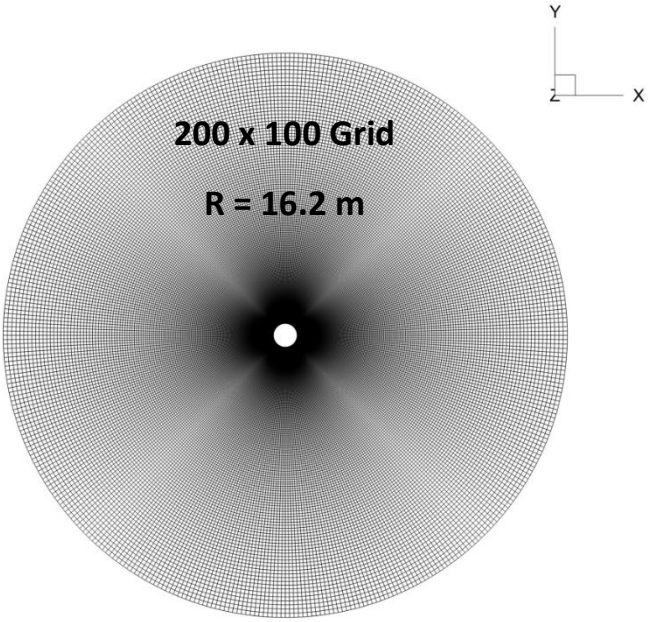

Figure 2: Overall Grid Structure

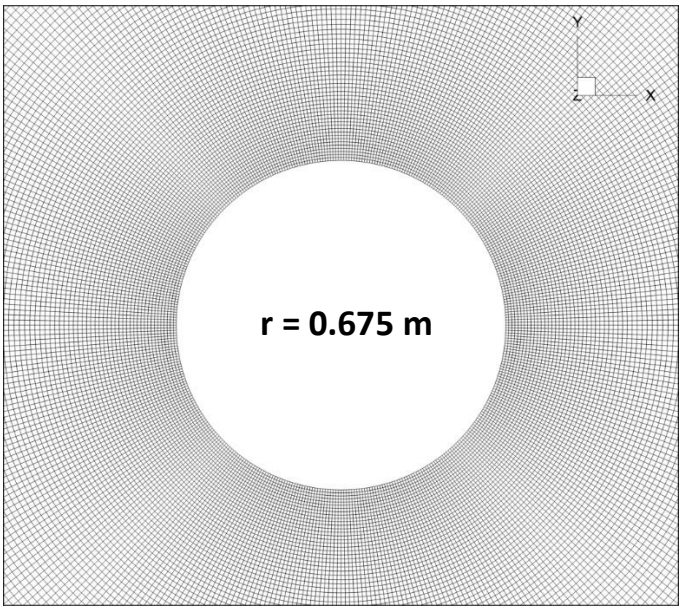

Figure 3: Close-Up Mesh

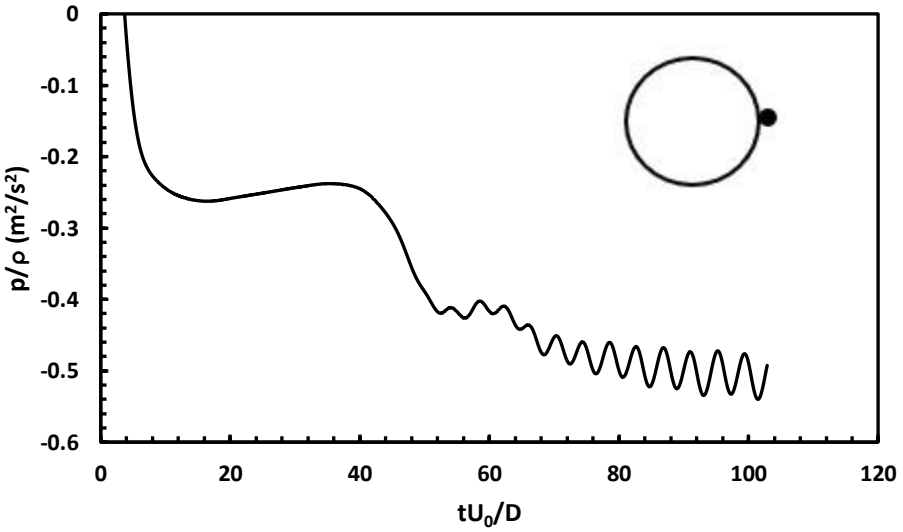

Figure 4: Early Periodic Base Pressure

Simulation Properties

υ = 0.0075 m^2/s

D = 1.35 m

U_0 = 1.11 m/s

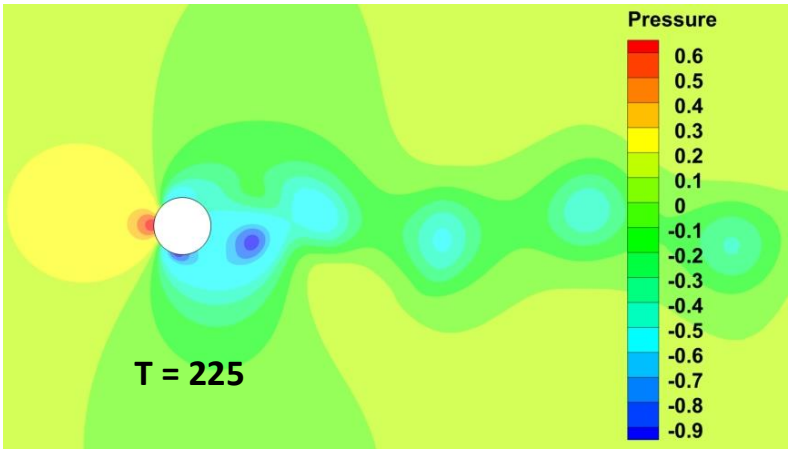

Figure 5: Vortex Street

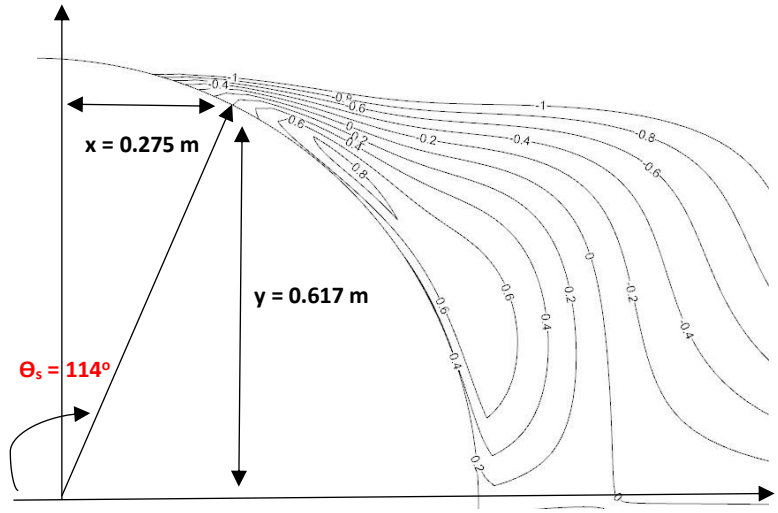

Figure 6: Θ_s Vorticity Contours

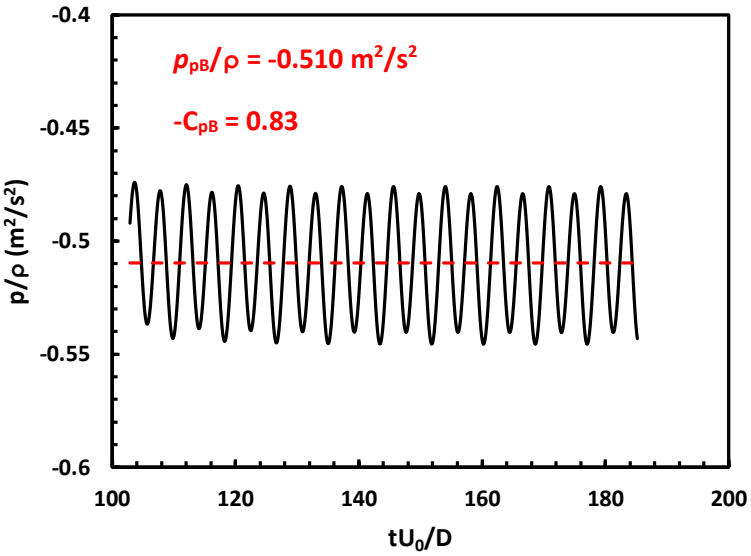

Figure 7: Full Periodic Base Pressure

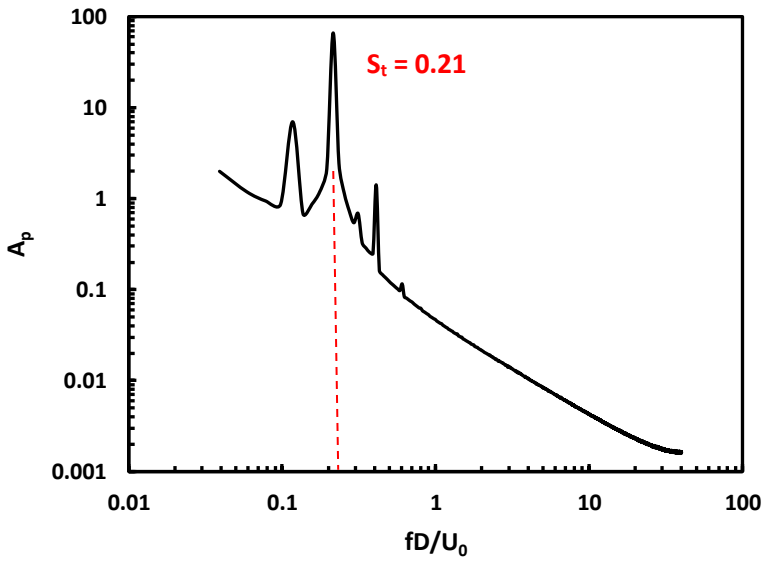

Figure 8: Fourier Transform of Base Pressure

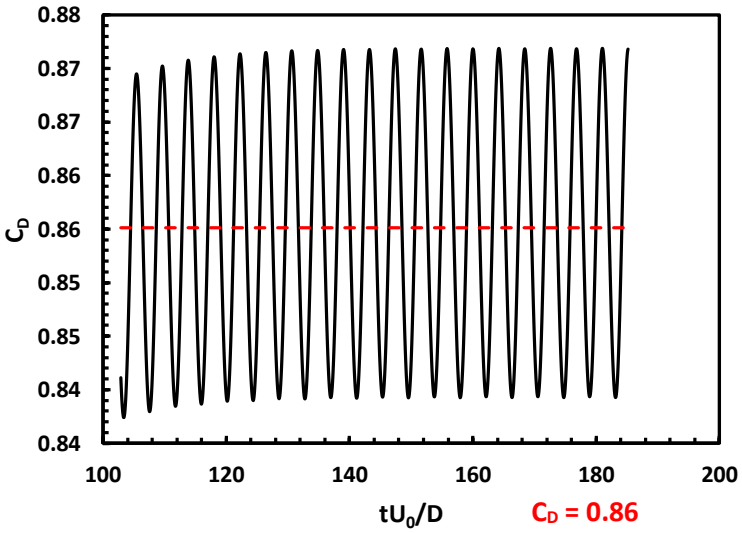

Figure 9: Coefficient of Drag

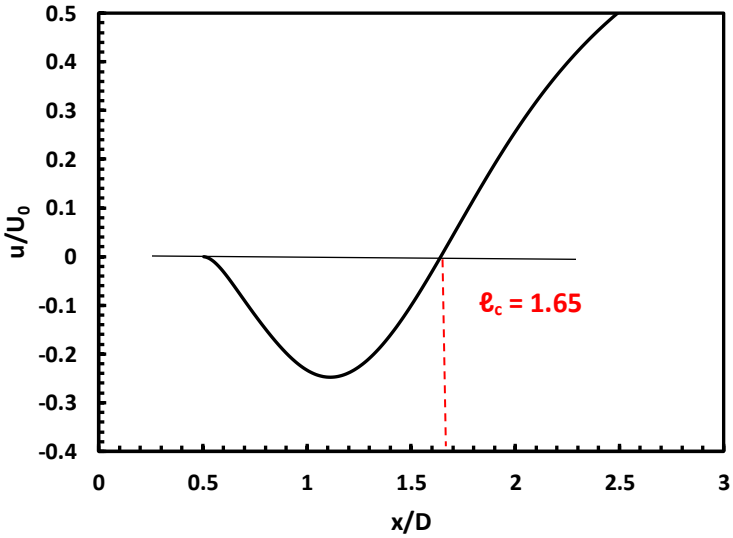

Figure 10: Bubble Length

Table 1: Laminar Cylinder Flow Parameters

Parameter	Experiments	Simulation
υ	-----	0.0075 m^2/s
D	-----	1.35 m
C_L	0	0.0042
C_D	1.3	0.86
S_t	0.182 ± 0.04	0.21
$-C_{pB}$	0.86	0.83
ℓ_c	1.4	1.65
Θ_s	115° ± 1°	114°